

Pion Production and Elastic Scattering in Antiproton-Proton Collisions at 6.94 BeV/c*

T. FERBEL,† J. A. JOHNSON, H. L. KRAYBILL, J. SANDWEISS, AND H. D. TAFT

Yale University, New Haven, Connecticut and Brookhaven National Laboratory, Upton, New York

(Received 22 March 1968)

We have studied nonstrange \bar{p} - p interactions observed in 7000 pictures of the 80-in. Brookhaven National Laboratory hydrogen bubble chamber exposed to an antiproton beam with a momentum of 6.94 BeV/c. The total cross section was measured to be 58.7 ± 2.8 mb, and the elastic interaction cross section 14.2 ± 1.2 mb. The elastic differential cross section for four-momentum transfers $(-t) \leq 0.3$ (BeV/c)² is well described by the exponential form $d\sigma_{el}/dt = (d\sigma/dt)_{t=0} e^{bt}$, where $b = 13.1 \pm 1.1$ (BeV/c)⁻². The single-pion production cross section is 4.0 ± 0.9 mb. This channel proceeds 70% through resonance formation. $N^*(1238)$ isobar and anti-isobar formation dominates pion production in four- and six-pronged events; the double-isobar formation cross section in the final state $p\pi^+\bar{p}\pi^-$ is 1.35 ± 0.2 mb. Isobar production was observed to be consistent with the predictions of a dominant one-particle-exchange process. The pion-annihilation process, which has a cross section of 25 ± 5 mb, shows substantial pion resonance formation.

I. INTRODUCTION

IN this paper we report the results of an investigation of antiproton-proton collisions which involved final states containing pions and/or nucleons exclusively. This experiment, which used the Brookhaven National Laboratory (BNL) Alternating Gradient Synchrotron (AGS) in conjunction with the 80-in. hydrogen bubble chamber, is part of a collaborative Yale-BNL study of \bar{p} - p interactions; preliminary results have been reported.¹ We have measured 3000 two-pronged events, 1800 four-pronged events, and 1800 six-pronged events.

After a brief description of the analysis procedures, we present in Sec. II a study of the elastic interactions. Section III summarizes our results for the single-pion production channels. Multimeson production in non-annihilation events as seen in four- and six-pronged events and especially double isobar [$N^*(1238)$] production are discussed in Sec. IV. In Sec. V, results of preliminary investigations into multipion annihilations are given.

The beam particles were taken at 7° off a 2 in. (long) \times 0.1 in. (high) aluminum target installed at the AGS I-10 position. There were approximately 10 antiprotons per pulse entering the chamber.² Seven thousand photo-

graphs of the bubble chamber were scanned for all events using orthodox scanning techniques. Conventional measuring machines were connected on-line to a DEC PDP-1 computer which served as a measurement-quality monitoring device.³

From the known energy and measured range of 33 stopping muons from the decays of stopping π^+ mesons, the liquid-hydrogen density was found to be 0.062 ± 0.003 g/(cm).³ From a study of the observed width of the momentum spectrum for 900 incident antiprotons tracks, the setting error was found to be 75μ .⁴ A sample of 110 δ rays with electron momenta in excess of 30 MeV/c was used to estimate the beam purity. This was done by comparing the experimental momentum spectrum with the known differential collision probability for charged particles of different mass on electrons.⁵ The measured contamination was $(5 \pm 1)\%$ and was consistent with the assumption that all beamlike impurities were muons. The beam momentum as determined from kinematic fitting was found to be 6.94 ± 0.04 BeV/c, with a spread of 1.5%.

The measured $\bar{p}p$ total cross section of 58.7 ± 2.8 mb is consistent with more precise determinations.⁶ Table I contains a summary of the major production cross sections.

* Part of this work was submitted by J. A. Johnson in partial fulfillment of the requirements for the Ph.D. degree at Yale University, 1965. Research supported in part by the U. S. Atomic Energy Commission under Contract No. Yale-2726-519.

† Present address: University of Rochester, Rochester, N. Y.

¹ Preliminary results on the data reported in this paper may be found in T. Ferbel, A. Firestone, J. Johnson, J. Sandweiss, and H. Taft, *Nuovo Cimento* **38**, 12 (1965); **38**, 19 (1965). Results on hyperon production may be found in C. Y. Chien, J. Lach, J. Sandweiss, H. D. Taft, N. Yeh, Y. Oren, and M. Webster, *Phys. Rev.* **152**, 1171 (1966).

² Some details concerning the design, construction, and operation of the 80-in. BNL bubble chamber and the separated antiproton beam may be found in J. G. Androulakis, J. A. Bamberger, D. P. Brown, H. O. Courtney, B. B. Culwick, J. J. Diener, W. B. Fowler, C. L. Goodzeit, J. Hanush, E. L. Hart, H. Houtsager, J. E. Jensen, D. A. Kassner, D. T. Liverios, R. I. Louttit, S. C. Mo, T. W. Morris, R. B. Palmer, P. A. Pion, R. R. Rau, R. Rutan, R. P. Shutt, H. H. Sondericker, A. M. Thorndike, W. A. Tuttle, I. J. Winters, H. Woelfel, D. H. Wright, S. S. Yamamoto, F. Anderson, H. W. Courant, and H. L. Kraybill, *Nucl. Instr. Methods* **20**, 100 (1962); I. Skillicorn and M. Webster, Internal Report Brook-

haven National Laboratory Report No. BNL H-10, 1962 (unpublished).

³ For a discussion of this technique, see H. D. Taft and P. Martin, in *Proceedings of the Twelfth International Conference on High-Energy Physics, Dubna, 1964* (Atomizdat, Moscow, 1965), Vol. 2, p. 390.

⁴ The measuring error in the momentum can be expressed, neglecting the inherent spread in the beam, as a function of particle momentum, particle velocity, bubble-chamber magnetic field, track length, number of measured points on the track, and the setting error. When the measuring accuracy is determined, the setting error can be calculated; see J. A. Johnson III, Ph.D. thesis, 1965, Yale University (unpublished).

⁵ For the detailed procedure see T. Ferbel *et al.*, *Phys. Rev.* **137**, B1250 (1965); also, Tohoku University Report No. TUHEL-5, 1967 (unpublished).

⁶ W. Galbraith, E. Jenkins, T. F. Kycia, B. A. Leontic, R. H. Phillips, and A. L. Read, Brookhaven National Laboratory Report No. BNL-8744 (unpublished).

TABLE I. Major cross sections in $\bar{p}+p$ collisions at 6.94 BeV/c.

$\bar{p}+p \rightarrow 0$ prongs	1.4 ± 0.3 mb
2 prongs ^a	32.6 ± 2 mb
4 prongs	16.6 ± 1.5 mb
6 prongs	6.9 ± 0.8 mb
8 prongs	1.2 ± 0.5 mb
Total	58.7 ± 2.8 mb
2-prong/total ^a	$(55.6 \pm 2.2)\%$
4-prong/total	$(28.3 \pm 0.9)\%$
6-prong/total	$(11.8 \pm 0.5)\%$

^a This includes a 6.2-mb correction for small-angle elastic scattering losses.

II. ELASTIC INTERACTIONS

The χ^2 distribution, the distribution in the square of the missing mass, and the spectrum of deviations from coplanarity for the 835 elastic interactions found in the two-pronged event sample are given in Fig. 1. The tail of the χ^2 distribution is thought to have arisen from the influence of non-Gaussian errors in track parameter measurements for short tracks made by low-momentum protons. The spectrum of the missing mass squared is centered, as expected, near zero; the slight asymmetry observed here is caused by the systematic tendency of errors in momentum measurement to be larger than the associated errors in the determination of the energies.⁷ The observed deviations from coplanarity are shown to be centered on zero and Gaussian-distributed when each coplanarity is normalized to its calculated error.

The total elastic interaction cross section is 14.2 ± 1.2 mb. This number takes account of a 40% scanning loss for low-momentum-transfer events; the correction is made assuming an exponential form for the elastic scattering distribution at small angles. The observed elastic interactions comprised 31% of all two-pronged events measured. The extrapolated differential cross section at 0° is consistent with the assumption of no real part to the forward scattering amplitude. Be-

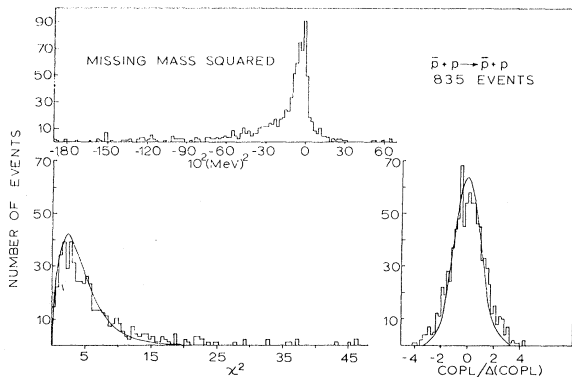


FIG. 1. χ^2 , missing mass squared, and coplanarity distributions for elastic interactions. The χ^2 spectrum is compared with the theoretical four-constraint χ^2 curve, using a 1.3 expansion factor on the horizontal scale. The coplanarity distribution is given in units of σ (standard deviation) and is compared with a Gaussian curve with $\sigma = 1$.

⁷ This point is elucidated in A. H. Rosenfeld and W. E. Humphrey, *Ann. Rev. Nucl. Sci.* **13**, 103 (1963).

cause of poor statistics, however, we cannot improve on the limit quoted in Ref. 8.

When the target nucleon is approximated by a purely absorbing disk of radius R and the fraction of the incident wave absorbed at impact parameter d is constant for $d \leq R$ and is zero for $d > R$, the elastic angular distribution for small $\theta_{c.m.}$ and large kR is⁹

$$\frac{d\sigma_{el}}{d\Omega} \sim \left[\frac{J_1(kR \sin \theta_{c.m.})}{\sin \theta_{c.m.}} \right]^2,$$

where k is the c.m. wave number. In Fig. 2, this prediction is compared with the data; a radius $R = 1.3$ F was found to give a satisfactory fit for $0.94 < \cos \theta_{c.m.} < 0.98$. The data do not clearly show any of the recently observed diffraction minima.¹⁰

A least-squares fit of the data shown in Fig. 2 was made to an exponential in t of the form

$$\frac{d\sigma_{el}}{dt} = \frac{k^2}{16\pi^2} \sigma_{tot}^2 e^{bt}$$

for values of $-t$ between 0.08 and 0.30 (BeV/c)². The best fit gave $b = 13.1 \pm 1.0$ (BeV/c)⁻² or $r = 1.4 \pm 0.1$ F.⁸ A study of $\ln(d\sigma_{el}/dt)$ versus $\ln(-t)$, as suggested by Serber,¹¹ showed these data to be consistent with

$$\left(\frac{d\sigma_{el}}{dt} \right) / \left(\frac{d\sigma_{el}}{dt} \right)_{t=0} \sim (-t)^{-4 \pm 1}$$

for $(-t) \geq 0.2$ (BeV/c)².

III. SINGLE-PION PRODUCTION

Cross sections for the reactions

$$\bar{p}+p \rightarrow \bar{p}+p+\pi^0, \quad (1)$$

$$\bar{p}+p \rightarrow p+\pi^-+\bar{n} \quad (2)$$

were determined from the distributions in the missing mass squared for all two-pronged events which did not give an acceptable fit to the elastic interpretation ($\chi^2 \geq 30.0$). Smooth-curve approximations to background contributions were extrapolated through the regions in missing mass squared where the signals from reactions (1) and (2) were expected. Clear evidence for single pion production was given by these procedures. Figure 3 displays the nucleon and pion angular distribution obtained from these events with pionlike and nucleonlike missing masses. Ionization studies of all two-pronged events which did not fit the elastic inter-

⁸ K. J. Foley, S. J. Lindenbaum, W. A. Love, S. Ozaki, J. J. Russell, and J. Yuan, *Phys. Rev. Letters* **11**, 503 (1963).

⁹ This is the usual optical model treatment. See S. Fernbach *et al.*, *Phys. Rev.* **75**, 1352 (1949); G. A. Smith *et al.*, *ibid.* **123**, 2160 (1961).

¹⁰ B. Barish, D. Fong, R. Gomez, D. Hartill, J. Pine, A. V. Tollestrup, A. Maschke, and T. F. Zipf, *Phys. Rev. Letters* **17**, 720 (1966); W. M. Katz, B. Forman, and T. Ferbel, *ibid.* **19**, 265 (1967).

¹¹ R. Serber, *Phys. Rev. Letters* **10**, 357 (1963).

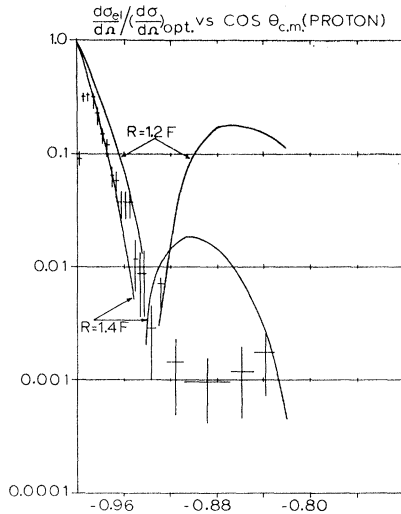
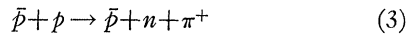


FIG. 2. Optical-model treatment: the black absorbing disk. The curves shown are the theoretical predictions for assumed values of the disk radius R .

pretations but which did fit ($\chi^2 \leq 6.0$) reactions (1) or (2) (or both) showed that the background is primarily due to kinematic ambiguities between reactions (1), (2), and (3). The measured cross sections for reactions (1) and (2) were 1.3 ± 0.3 and 1.1 ± 0.3 mb, respectively. It was not possible to measure the cross section for



due to poor mass resolution; since reactions (3) and (2) are equivalent under C invariance when neither the

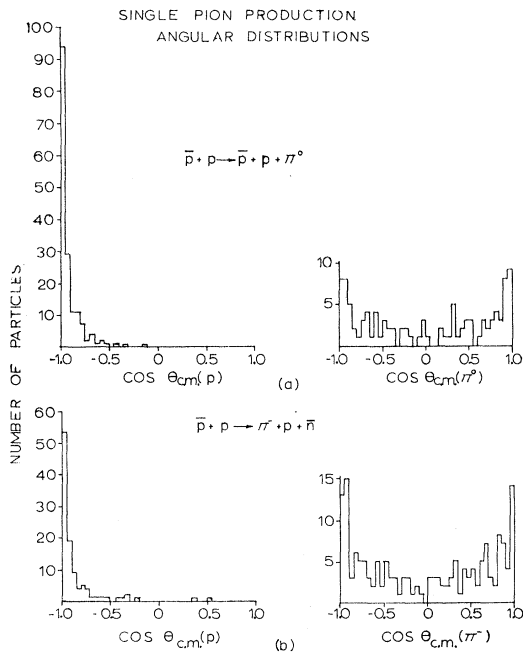


FIG. 3. Single-pion production angular distributions. In the $\bar{p}p\pi^0$ (a) and $\bar{p}p\pi^-$ (b) final states, the contamination was less than 8%.

TABLE II. Single-pion production.

Reaction	Cross section (mb)
$\bar{p} + p \rightarrow \bar{p} + p + \pi^0$	1.3 ± 0.3
$\bar{p} + p \rightarrow \bar{p} + n + \pi^0$	1.1 ± 0.3
$\bar{p} + p \rightarrow \bar{p} + p + \pi^-$	1.1 ± 0.3
$N^*(1238) + N$	1.25 ± 0.4
$N^*(1512) + N$	1.3 ± 0.4
$N^*(1688) + N$	

target nor the beam particles are polarized, their cross sections were equated. Table II contains a summary of single-pion production cross sections.

The diffractionlike nature of reactions (1) and (2) is indicated in Fig. 3. Nucleon production [i.e., proton production in (1) and (2)] in single-pion production data was reasonably well described for $-0.95 \leq \cos \theta_{c.m.} \leq -0.80$ by

$$\left[\frac{d\sigma}{d(\cos\theta)} \right] / \left[\frac{d\sigma}{d(\cos\theta)_{180^\circ}} \right] = \exp[-(1.35 \pm 3)(\cos\theta + 1)].$$

In reaction (1), 69% of all neutral pions were produced with $|\cos \theta_{c.m.}| \geq 0.5$. These reactions are clearly dominated by low four-momentum-transfer processes.

The effective masses (M) for the nucleon-pion and the antinucleon-pion pair were computed for each single-pair-production event. The results are given in Fig. 4. $M^2(p, \pi^0)$ and $M^2(p, \pi^-)$ are plotted as $M^2(N, \pi)$ and $M^2(\bar{p}, \pi^0)$ and $M^2(\bar{n}, \pi^-)$ are plotted as $M^2(\bar{N}, \pi)$. These Dalitz-plot distributions do not follow the pre-

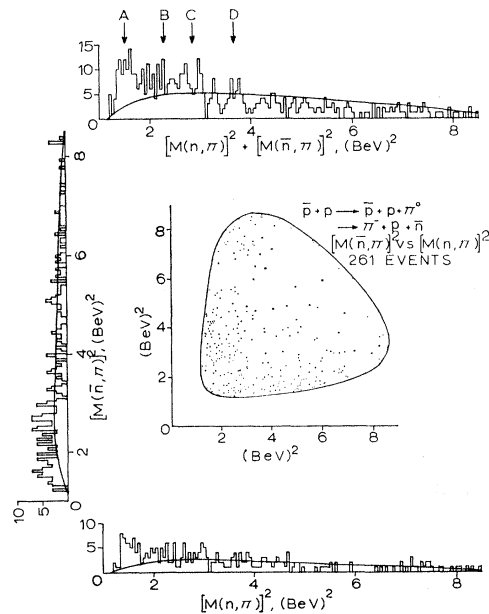


FIG. 4. Dalitz plot for single-pion production. Smooth curves are Lorentz-invariant phase-space predictions. The masses of $N^*(1238)$, $N^*(1512)$, $N^*(1688)$, and $N^*(1910)$ are indicated by the A, B, C, and D arrows, respectively.

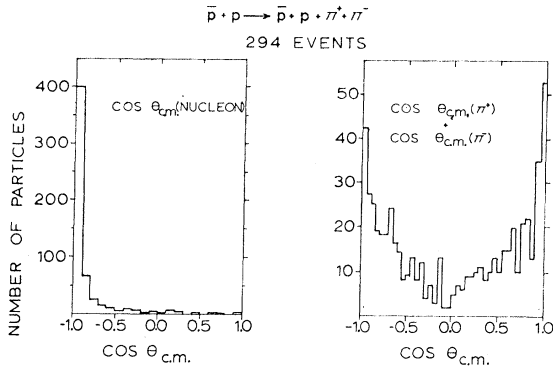


FIG. 5. Angular distributions for $\bar{p}+p \rightarrow \bar{p}+p+\pi^++\pi^-$. The nucleon angular distributions were combined using $\cos\theta_{e.m.}(\text{nucleon}) = \cos\theta_{e.m.}(\text{proton})$, $\cos\theta_{e.m.}(\text{nucleon}) = -\cos\theta_{e.m.}(\text{antiproton})$. No such reflection is made in the pion angular distribution.

dictions of Lorentz-invariant phase space. If all significant deviations from Lorentz-invariant phase space are interpreted as evidence for $N\pi$ resonance formation, 70% of single-pion production is seen to proceed via $N^*(1238)$, $N^*(1512)$, and $N^*(1688)$ production. Comparisons of the data from this experiment with that from experiments at lower \bar{p} energies¹² show continued prominence of $I = \frac{3}{2} \pi N$ resonance production. However, the percentage of the total cross section which proceeds via the single-pion-production channels has decreased.

IV. MULTIPION PRODUCTION

294 events were identified as examples of

$$\bar{p}+p \rightarrow \bar{p}+p+\pi^++\pi^- \quad (4)$$

The cross section for this reaction was 2.7 ± 0.2 mb. In this sample 98% of the events were unambiguously resolved through a study of observed track bubble densities. The angular distributions for these events are

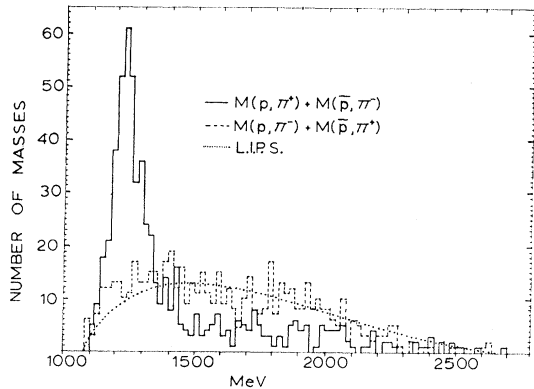


FIG. 6. Effective-mass distributions for $\bar{p}+p \rightarrow \bar{p}+p+\pi^++\pi^-$. The equivalent (N,π) final states are combined and compared with Lorentz-invariant phase space.

¹² (a) H. Dehne, E. Lohrmann, E. Raubold, P. Soding, M. Teucher, and G. Wolf, Phys. Rev. **136**, B843 (1964); (b) T. Ferbel, A. Firestone, J. Sandweiss, H. D. Taft, M. Gailloud, T. W. Morris, A. H. Bachman, P. Baumel, and R. M. Lea, *ibid.* **137**, B1250 (1965).

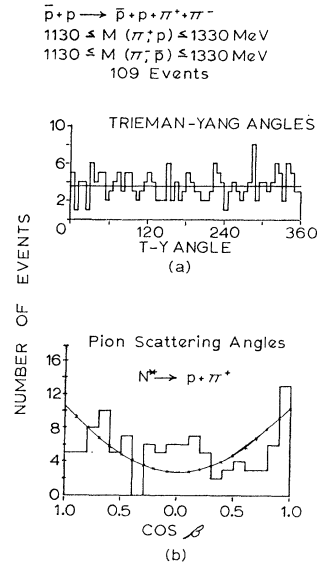


FIG. 7. (a) Treiman-Yang angle distributions. The distributions for N^* and \bar{N}^* are added since under C invariance, the N^* and \bar{N}^* production processes are identical and statistically independent. The straight line is for $d\sigma/d(TY\text{angle}) = \text{const.}$ (b) Pion scattering angle distribution. The virtual pion scattering angle is given by $\cos\beta = \pi_{N^*} \cdot N^*_{\text{lab}}$, where π_{N^*} is a unit vector along the π^+ direction in the N^* rest frame and N^*_{lab} is a unit vector along N^* direction in the laboratory system. The smooth curve is for $d\sigma/d\beta \sim (1+3\cos^2\beta)$.

shown in Fig. 5. Reaction (4) is dominated by low four-momentum transfers to the doubly charged πN system. Figure 6 shows evidence for strong $N^{*++}(1238)$ [and $\bar{N}^{*--}(1238)$] production, including the simultaneous production of $N^{*++}(1238)$ in the reaction

$$\bar{p}+p \rightarrow N^{*++}(1238) + \bar{N}^{*--}(1238). \quad (5)$$

No other resonances were observed clearly in reaction (4).

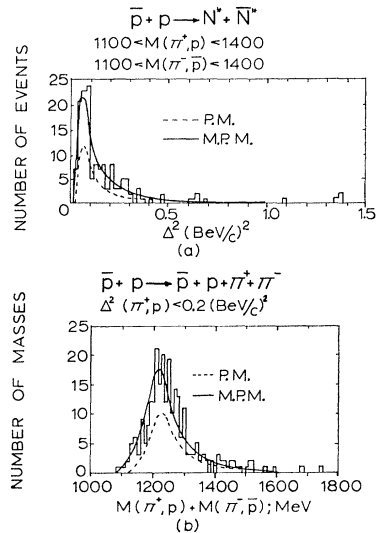


FIG. 8. Comparisons with OPE models. The theoretical curves shown are the predictions of the pole model (P.M.) and modified pole model (M.P.M.).

For reaction (5) which accounts for about 50% of reaction (4), and for those examples of reaction (4) which occur with low four-momentum transfers $\Delta^2(p\pi^+)$, the dominant production process at lower energies was thought to be one-pion exchange (OPE).¹²

We have investigated the applicability of various one-particle exchange hypotheses to our data.¹³⁻¹⁸ For a OPE mechanism, the distribution in the Treiman-Yang angles is expected to show isotropy¹⁵; Fig. 7 shows this expectation to be well satisfied for reaction (5). For $J = \frac{3}{2}$, $J_z = \frac{1}{2}$ isobar decay, without final-state interferences, the distribution in pion scattering angles is expected to show a $(1+3\cos^2\beta)$ behavior. Figure 7 indicates that within the statistical uncertainties this is also satisfied.

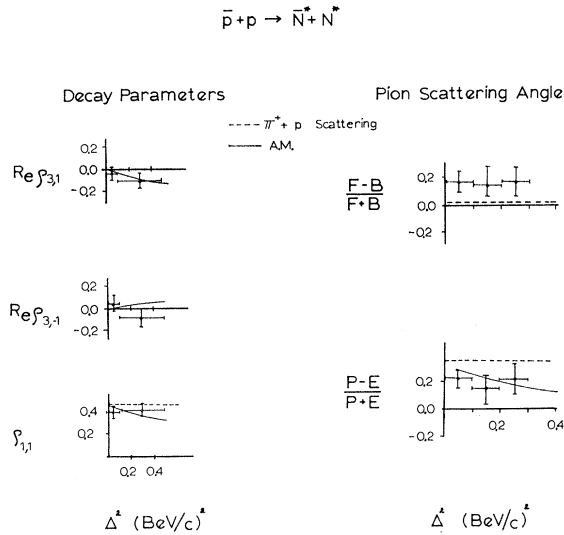


FIG. 9. Comparisons with OPE models. Smooth curves are predictions of the absorptive model (A.M.). (See Ref. 20.) F , B , P , and E specify $\cos\beta \geq 0.0$, $\cos\beta \leq 0$, $|\cos\beta| \geq 0.5$ and $|\cos\beta| \leq 0.5$ respectively, where β is the scattering angle of the virtual pion. [See Fig. 7(b).] The ρ 's are elements of the density matrix. The dashed lines were drawn for experimental (real) π^+p scattering (ignoring Coulomb effects).

If the fact that the exchanged pion is off the mass shell is ignored, then the prediction of the pole model (P.M.) are obtained.¹⁶ In the modified pole model (M.P.M.) empirical form factors for the pion propagator and for off shell scattering at the interaction vertices are prescribed which, once determined, should be

¹³ The importance of nucleon isobar formation in high-energy interactions has been emphasized by R. M. Sternheimer and S. J. Lindenbaum, Phys. Rev. **105**, 1874 (1957); Phys. Rev. Letters **5**, 24 (1960); and Phys. Rev. **123**, 333 (1961).

¹⁴ S. D. Drell, Rev. Mod. Phys. **33**, 458 (1961) gives a review of pole models.

¹⁵ See S. B. Treiman and C. N. Yang, Phys. Rev. Letters **8**, 140 (1962).

¹⁶ F. Salzman and G. Salzman, Phys. Rev. **121**, 154 (1961).

¹⁷ See E. Ferrari, Nuovo Cimento **30**, 240 (1963); E. Ferrari and F. Selleri, *ibid.* **27**, 1450 (1963).

¹⁸ Many authors have contributed to these developments. See J. D. Jackson, Rev. Mod. Phys. **37**, 484 (1965) for references to several earlier articles and a review of absorptive-model techniques.

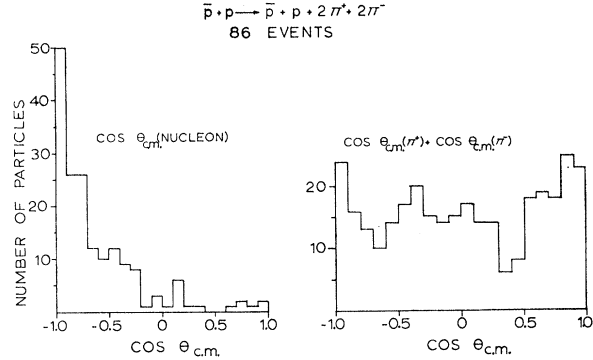


FIG. 10. Angular distributions for $\bar{p}+p \rightarrow \bar{p}+p+2\pi^++2\pi^-$. (See Fig. 5 for conventions used.)

“universal” in application.¹⁷ In the absorption model (A.M.), quasi-two-body final states are treated in terms of the strong absorptive processes in the entrance and exit channels arising from the presence, at high energies, of numerous competing open channels.¹⁸ Evaluations of the predictions of these models for reaction (5) were made in terms of predicted total and differential cross sections and in terms of angular correlations.

In Fig. 8 the $\Delta^2(p,\pi^+)$ spectrum for events with $M(p,\pi^+)$ and $M(\bar{p},\pi^-)$ between 1100 and 1400 MeV and the effective mass spectrum of π^+p and $\pi^-\bar{p}$ combinations for $\Delta^2(p,\pi^+) < 0.2$ (BeV/c)² are given. The absolute predictions of the P.M. and the M.P.M. are also shown.¹⁹ The cross-section prediction of the A.M. is too large by a factor of about 5.²⁰ The importance of

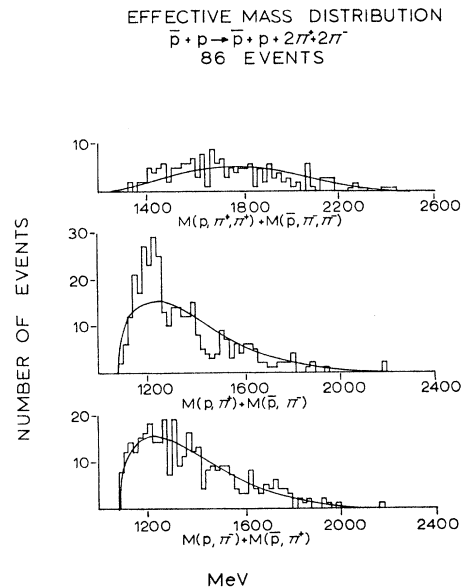


FIG. 11. Effective-mass distributions for $\bar{p}+p \rightarrow \bar{p}+p+2\pi^++2\pi^-$. The equivalent (N,π) and (N,π,π) final states are combined and compared with Lorentz-invariant phase space.

¹⁹ There are no free parameters in these predictions. See Refs. 12(b) and 21.

²⁰ We are grateful to B. E. Y. Svensson for generously providing us the unpublished density-matrix elements relevant to these studies of angular correlations in $\bar{p}+p \rightarrow N^*+\bar{N}$. See Ref. 21 for a comparison with lower energies.

TABLE III. Multipion production.

Reaction	Cross section (mb)
$\bar{p} + p \rightarrow \bar{p} + p + \pi^+ + \pi^-$	2.7 ± 0.3
$\bar{p} + p + 2(\pi^+ + \pi^-)$	0.26 ± 0.04
$\bar{p} + p + \pi^+ + \pi^- + \pi^0$	1.3 ± 0.3
$\bar{p} + p + 2(\pi^+ + \pi^-) + \pi^0$	0.14 ± 0.03
$N^{*++}(1238) + \bar{N}^{*-}(1238)$	1.35 ± 0.2
$\bar{N}^*(1238) + \bar{p} + \pi^-$	0.54 ± 0.3
$\bar{N}^*(1238) + \bar{p} + \pi^-$	0.54 ± 0.3
$\bar{N}^*(1238) + \bar{p} + 2\pi^+ + \pi^-$	0.21 ± 0.06
$\bar{N}^*(1238) + \bar{p} + 2\pi^- + \pi^+$	0.21 ± 0.06
$\bar{N}^*(1238) + \bar{p} + \pi^- + \pi^0$	0.44 ± 0.2
$\bar{N}^*(1238) + \bar{p} + \pi^+ + \pi^0$	0.44 ± 0.2
$\bar{p} + \pi^- + \pi^+ + \pi^- + \bar{n}$	< 1.6
$\bar{p} + \pi^+ + \pi^+ + \pi^- + \bar{n}$	< 1.6
$\bar{p} + \pi^+ + \pi^+ + 3\pi^- + \bar{n}$	< 2.0
$\bar{p} + \pi^- + \pi^- + 3\pi^+ + \bar{n}$	< 2.0

off-mass-shell corrections in reaction (5) is clearly shown in Fig. 9, where isobar decay correlations and pion scattering angles are examined.²⁰ One can conclude from Figs. 8 and 9 that although the pole models satisfactorily predict over-all features, careful considerations of absorptive processes are required in order to explain some details of this reaction in terms of the OPE mechanism.²¹

The cross section for the reaction

$$\bar{p} + p \rightarrow \bar{p} + p + 2\pi^+ + 2\pi^- \quad (6)$$

IDEOGRAM OF THE SQUARE OF THE MISSING MASS

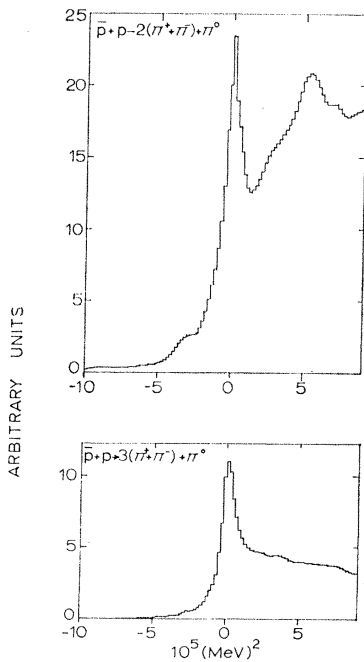


FIG. 12. Missing-mass-squared distributions for one-constraint annihilations. π^0 production in these events is evidenced by the Gaussian-shaped clustering, above the background, at the π^0 mass.

²¹ These results and further studies of isobar-anti-isobar pair production from 3 to 7 BeV/c are discussed in T. Ferbel, Bull. Am. Phys. Soc. 10, 585 (1965); Yale University Report, 1965 (unpublished).

MISSING MASS DISTRIBUTION

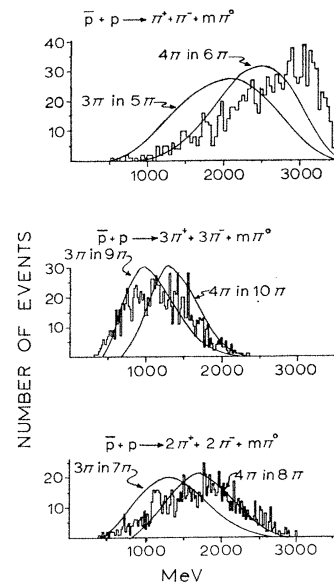


FIG. 13. Missing-mass spectra for annihilation candidates. The smooth curves are the predictions of Lorentz-invariant phase space.

is 0.26 ± 0.04 mb. The production angular distributions for the 86-event sample are shown in Fig. 10.

Prominent production of the $N^*(1238)$ [and $\bar{N}^*(1238)$] isobar is again observed in reaction (6). From Fig. 11, which shows the $M(p, \pi^+)$ and $M(\bar{p}, \pi^-)$ effective masses, we conclude that the data are consistent with at least one $N^*(1238)$ or $\bar{N}^*(1238)$ in every event. No other resonance production is observed. An examination of the three-body triply charged mass spectrum of πN^* events showed no evidence for πN^* resonance formation.²²

TABLE IV. Annihilation cross sections. \bar{m} is the average number of π^0 's missing.

Reaction	Cross section (mb)
2-prong	
$\bar{p} + p \rightarrow \pi^+ + \pi^-$	< 0.012
$2\pi^+ + 2\pi^-$	0.054 ± 0.02
$3\pi^+ + 3\pi^-$	0.216 ± 0.035
$\pi^+ + \pi^- + \pi^0$	< 0.29
$2(\pi^+ + \pi^-) + \pi^0$	0.42 ± 0.1
$3(\pi^+ + \pi^-) + \pi^0$	1.2 ± 0.1
$\pi^+ + \pi^- + m\pi^0$ ($\bar{m}=3$)	10.0 ± 1.0
$2(\pi^+ + \pi^-) + m\pi^0$ ($\bar{m}=3.4$)	10.5 ± 1.5
$3(\pi^+ + \pi^-) + m\pi^0$ ($\bar{m}=3.0$)	3.9 ± 0.5
$\rho^0\pi^0$	< 0.025
$\rho^0 + \pi^+ + \pi^- + \pi^0$	0.07 ± 0.03
$\rho^\pm + 3\pi$ (4-prong)	0.21 ± 0.09
$\omega^0 + \pi^+ + \pi^-$	< 0.04
$\rho^0 + 2(\pi^+ + \pi^-)$	0.09 ± 0.03
$\rho^0 + 2(\pi^+ + \pi^-) + \pi^0$	0.40 ± 0.07
$\rho^\pm + 5\pi$ (6-prong)	0.10 ± 0.03
$\omega^0 + 2(\pi^+ + \pi^-)$	0.10 ± 0.03

²² This would be the $I=\frac{3}{2}, J=\frac{5}{2} \pi N^*$ resonance, discussed for example, in H. Harari and H. J. Lipkin, Phys. Rev. Letters 13, 345 (1964); R. H. Dalitz, in *Proceedings of the Athens Topical Conference on Recently Discovered Resonant Particles, Athens, Ohio, 1963*, edited by B. A. Muncie and L. J. Gallagher (Ohio University Press, Athens, Ohio, 1963).

Nonannihilation final states with one missing neutral particle in four- and six-pronged events were too few in number for detailed studies. Cross sections were determined by examination of the missing mass distributions for all events which made no four-constraint fits (i.e., all events which could not be successfully interpreted assuming only charged particles in the final state) and by ionization studies on selected small samples of events. This yielded cross section for

$$\bar{p} + p \rightarrow \bar{p} + p + k(\pi^+ + \pi^-) + \pi^0, k = 1, 2$$

of 1.3 ± 0.3 and 0.14 ± 0.03 mb for $k=1$ and $k=2$, respectively. Prominent $N^*(1238)$ production for $k=1$ was also observed. Upper limits on the cross section for

$$\bar{p} + p \rightarrow \begin{cases} p + \pi^- + \pi^+ + \pi^- + \bar{n} \\ \bar{p} + \pi^+ + \pi^+ + \pi^- + n \end{cases}$$

and

$$\bar{p} + p \rightarrow \begin{cases} p + \pi^+ + \pi^+ + 3\pi^- + \bar{n} \\ \bar{p} + \pi^- + \pi^- + 3\pi^+ + n \end{cases}$$

were 1.6 and 2.0 mb, respectively. In Table III, a summary is given of all multipion production cross sections measured.

V. ANNIHILATIONS

A kinematic fit to the reactions

$$\bar{p} + p \rightarrow k(\pi^+ + \pi^-), k = 1, 2, 3$$

was attempted for all two-, four-, and six-pronged events, respectively. The fit was deemed acceptable when the χ^2 was ≤ 40.0 . From studies of ambiguities between one-constraint (a missing π^0) and four-constraint fits it was determined that the background which arose from ignoring all one-constraint fits, when a four-constraint fit was successful, was less than 5%. No events were found which made the fit for $k=1$, giving a cross section upper limit of 0.012 mb. For $k=2$, and $k=3$, the cross sections were found to be 0.054 ± 0.02 and 0.216 ± 0.03 mb, respectively.

Every event was considered to be a candidate for

$$\bar{p} + p \rightarrow k(\pi^+ + \pi^-) + m\pi^0$$

if the event had no acceptable four-constraint fits. In $\bar{p} + p$ collisions with an unpolarized beam and target, charge-conjugation invariance requires symmetric distributions of the cosine of the $m\pi^0$ systems's production angle in the c.m. system.²³ This criterion was used in conjunction with the studies of the missing-mass squared distributions to obtain estimates of cross sections. For $k=m=1$ a cross-section upper limit of 0.29 mb was determined. Ideograms of the missing mass squared for $k=2$ and $k=3$ are given in Fig. 12. The deduced cross sections for $m=1$ are 0.4 ± 0.1 and 1.2 ± 0.2 mb for $k=2$ and $k=3$, respectively. Cross-section

²³ A. Pais, Phys. Rev. Letters 3, 242 (1959).

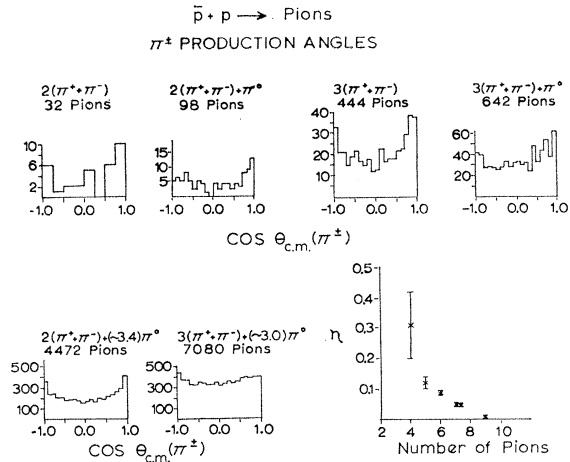


FIG. 14. Charged-pion-production angles in annihilations; c.m. production angles are plotted with respect to the incoming antiproton beam according to the prescription: $\cos\theta_{c.m.}(\pi^\pm) = \cos\theta_{c.m.} \times (\pi^-)$, $\cos\theta_{c.m.}(\pi^\pm) = -\cos\theta_{c.m.}(\pi^+)$. The decrease in forward-backward asymmetry with increasing pion multiplicity is indicated by $\eta = (F-B)/(F+B)$.

determinations contain corrections for strange-particle production.²⁴

The cross sections for multi- π^0 production annihilations ($m \geq 2$) were determined by fitting appropriate Lorentz-invariant phase-space predictions to the missing-mass spectra. Some examples of the curves used are given in Fig. 13. A background in these events from

$$\bar{p} + p \rightarrow k(\pi^+ + \pi^-) + n + \bar{n}$$

did not affect the fitting for four- and six-pronged events since the fitting was confined to events with

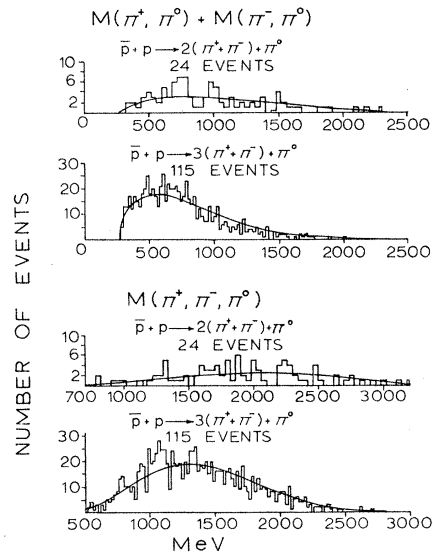


FIG. 15. Effective-mass spectra in annihilations. $M(\pi^\pm, \pi^0)$ and $M(\pi^+, \pi^-, \pi^0)$ are compared to Lorentz-invariant phase-space predictions for four- and six-pronged annihilations.

²⁴ N. Yeh and C. Y. Chien (private communication).

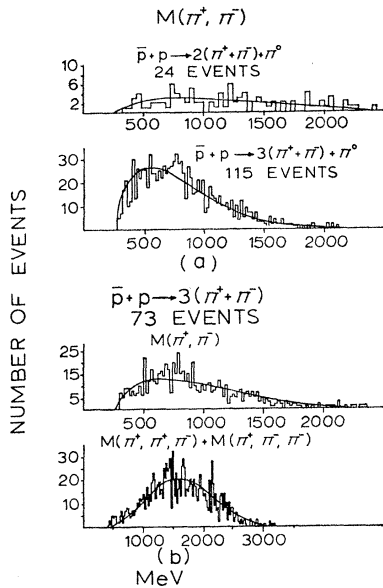


FIG. 16. Effective-mass spectra in annihilations. (a) $M(\pi^+, \pi^-)$ is given for four- and six-pronged annihilations with missing π^0 's; (b) six-pronged annihilations with no missing neutrals.

missing masses equal to or less than 1700 MeV. In two-pronged events, the background from nonannihilations with one or more charged nucleons which could not be eliminated is not negligible and has probably caused the cross section for these channels to be overestimated.

Cross sections, along with average multiplicities for all annihilation reactions, are given in Table IV. Although the annihilation cross section is diminishing with energy²⁵ it still accounts for a sizeable portion of the total cross section even at 7 BeV/c.

An examination of c.m. production angles for charged pions, shown in Fig. 14, suggests that forward-backward peaking in annihilations may increase with incident \bar{p} energies.²⁵ This effect, along with high c.m. energies (with respect to predictions from Lorentz-invariant phase space) and highly collimated c.m. momenta for charged particles, indicates that the annihilation process is partially peripheral. We also observed that asymmetries in pion correlation angles follow phase-space predictions; differences observed at lower \bar{p} energies²⁶⁻²⁷ between like pions and unlike pions have diminished.

All annihilation final states were examined for multipion resonance production. Figures 15 and 16 show the effective-mass configurations which would indicate ω and ρ production. The cross sections are given in

²⁵ T. Ferbel, A. Firestone, J. Sandweiss, H. Taft, M. Gaillard, T. Morris, W. Willis, A. Bachman, P. Baumel, and R. Lea, Phys. Rev. **143**, 1096 (1966), and references therein.

²⁶ J. A. Danysz and A. Shapira, CERN Report No. 65-8 (unpublished).

²⁷ G. Goldhaber, S. Goldhaber, W. Lee, and A. Pais, Phys. Rev. **120**, 300 (1960).

TABLE V. Summary of all cross sections measured in present experiment.

Reaction	Cross section (mb)
$\bar{p} + p \rightarrow \bar{p} + p$	14.2 ± 1.2
$\rightarrow \bar{p} + p + \bar{p} + p$	≤ 0.015
\rightarrow annihilation (av. multiplicity 7.0)	25 ± 5
\rightarrow pion production	14 ± 4
\rightarrow strange-particle production ^a	5 ± 1.5
\rightarrow pion resonances ^b	1.0 ± 0.5
Total	58.7 ± 2.8

^a N. Yeh and C. Y. Chien (private communication).

^b The ratio (pion resonances/fittable pionic annihilation states) = 0.6.

Table IV. Although it seems that total pion-resonance production is not decreasing with increasing \bar{p} energy, accurate cross-section determinations are difficult to make with the available statistics.

VI. CONCLUSIONS

Table V gives a summary of all cross sections measured in this experiment. In this section, some conclusions will be drawn from these results.

First, peripheral-type mechanisms seem to be important for all interactions. This is clearly indicated in the angular distributions which show predominantly forward-going antiprotons and negative pions in the final state. This is especially evident in the case of double isobar production [$N^*(1238)$] in the four-pronged events.

Secondly, the importance of the production of multipion and pion-nucleon resonance emerges in these data. More than 75% of all nonannihilation four- and six-pronged events, without neutral pion production, showed pion-nucleon resonance production. More than 75% of single-pion production proceeds through a resonance production channel. Multipion resonance production is prominent in the annihilation channels even though detection of these final states is difficult.

Finally, the elastic interaction displays a characterizing radius length which is roughly 1.4 F. Although some of the theoretical predictions for elastic interaction parameters are successful, no over-all conclusions can be drawn in this regard.

ACKNOWLEDGMENTS

It is a pleasure to acknowledge the many contributions to this experimental effort made by members of the AGS staff and the Yale and BNL bubble chamber groups. The computing center staffs at Yale and New York Universities provided assistance and cooperation throughout all phases of data analysis. We would also like to thank Dr. B. Svensson, Dr. F. Selleri, and Dr. E. Ferrari for many interesting discussions regarding peripheral models. Finally, we thank Dr. A. Firestone for his help in the early stages of this experiment.